JEE Journal of Ecological Engineering

Journal of Ecological Engineering 2024, 25(10), 209–223
https://doi.org/10.12911/22998993/192140
ISSN 2299–8993, License CC-BY 4.0

Received: 2024.07.31
Accepted: 2024.08.21
Published: 2024.09.01

Efficient Removal of As(III) and As(V) from Contaminated Water Using Novel Synthesized Porous Geopolymer

Abdul Qadeer[1*], Khadija Qureshi[1], Shaheen Aziz[1], Imran Nazir[1]

[1] Department of Chemical Engineering, Mehran University of Engineering and Technology, Jamshoro, Pakistan
* Corresponding author's e-mail: abdul.qadeer@admin.muet.edu.pk

ABSTRACT

Millions of people all over the globe are highly affected by arsenic toxicity. The aim of current study was to synthesis of porous geopolymer for effective arsenic As(III) and As (V) sequestration from aqueous solution. In addition to that morphological and chemical analysis of adsorbent was conducted by scanning electron microscopy (SEM), energy dispersion x-ray spectroscopy (EDX) and fourier transform infrared radiations (FTIR) and BET. FTIR results reveled the formation of Si–O–Si and Si–O–Al bonds which confirmed the construction of geopolymer. SEM images represent that adsorbent has a regular, spherical and interconnected porous structure with greater specific surface area and porosity. The best removal efficiency of As(III) was 62% at optimized operating conditions of pH 5–6, adsorbent dose 1 gm and initial concentration of pollutant 50 ppb, however As(V) removal efficiency was 94% at optimized operating conditions of pH 7–9, adsorbent dose 1 gm and initial concentration of pollutant 50 ppb. The experimental results was validated by renowned Freundlich adsorption isotherm model and peuso second order kinetic model. The correlation coefficient R^2 value obtained was 0.968 and 0.949 for As(III) and As(V) Freundlich model respectively. While R^2 was 0.98 and 0.99 for pseudo second order kinetic model. It was determined from R^2 that experimental results fitted well to Freundlich adsoprtion isotherm model and pseudo second order kinetic model. The results shows that adsorption capacity for As(III) and As(v) is greater than adsorption capacity obtained by other researchers using various adsorbents.

Keywords: arsenic, adsorbent, water treatment, waste water, porous geopolymer.

INTRODUCTION

Water is the vital components for the survival of life on Earth [Siyal et al., 2018]. Only around 2.5% of the world's total water is pure water from 71% [Khatri and Tyagi, 2015]. The fresh water resources containing rivers, lakes, ponds, ground water, and other streams [Xu et al., 2020), due to growing industrialization and modernization have had a negative impact on clean water resources [Christopher et al., 2023: Asia and Sarker, 2021]. About 230 millions of people around the world are currently suffering from arsenic-related diseases, which can be traced back to the utilization of arsenic-affected groundwater. Along with other countries more than 100 countries including Mexico, Taiwan, Argentina, Canada, Hungary, Japan, Bangladesh, India, New Zealand and Pakistan also has concentration of Arsenic above 10 ppb limit set by WHO [Shridhar et al., 2023]. Natural weathering processes, biological activity, geochemical processes, volcanic emissions, and other anthropogenic activities responsible for the mobilization of arsenic [Chung et al., 2014]. The United State Environmental Protection Agency has designated inorganic arsenic as the number one priority pollutant, with trivalent arsenic being nearly 70 times more hazardous than oxidized pentavalent inorganic arsenic compounds approximately 100 times more poisonous than organic. The International Agency for Research on Cancer has categorized Group 1 carcinogenic. Arsenic can cause severe effects, such as kidney injury, nausea and vomiting diarrhea, an inability to concentrate, disturbances in the neurological and cardiovascular systems' operations, or even mortality in extreme environment. Prolonged Arsenic exposure with low concentration or short term with higher concentration in water and food increases the risk of developing skin, kidney, bladder, and lung cancers. Joseph Davidovits was the one who invented geopolymer in 1970s, the synthesis was carried out by poly-condensation polymerization reaction of aluminum silicate containing materials in the existence of alkali activating solution [Davidovits, 2002; Davidovits, 1994]. Geopolymers encompass possess a diverse potential applications such as, compressive strength [Tang et al. 2023: Ahmed et al., 2022], adsorbents [Rickard and Van Riessen 2014], fire resistance [Sekkal and Zaoui, 2023] pH regulator [Novais et al., 2020], reducing CO_2 emission [Das et al., 2022] catalysts or catalytic supports [Al - Zeer and Mackenzie, 2019; Sharma et al., 2015; Alzeer, Zhu et al., 2022; Supamathanon et al., 2021; Alzeer et al., 2020; Rocca et al., 2021], better acid, sulfate and heat resistance [Caiet al., 2014; Wang et al., 2021; Singh et al., 2015; Łach et al., 2021; Khan et al., 2023; Ali et al., 2017], waste encapsulation [Kupwade-Patil et al., 2014; Guzmán-Carrillo et al., 2021; Grba et al., 2023], construction materials [Shehata et al., 2022; Zhang et al., 2014; Pacheco-Torgal et al., 2008; Ng et al. 2018] restoration and conservation [Ricciotti et al., 2022]. Chitosan-coated biosorbent [Grba et al., 2023], Poly acrylonitrile fiber and iron ore adsorbents [Bhatti et al., 2020], iron oxide coated geopolymer [Thakur and Armstrong, 2021], Iron oxide-modified nanoporous geopolymers [Medpelli et al., 2015], iron oxide-coated fungal biomass [Pokhrel and Viraraghavan, 2008], rice husk ash adsorbent modifed by iron oxide [Javed et al., 2023]. However, these adsorbents have a number of drawbacks, such as limited removal efficiency, no regeneration possibility, the impurities and sluggish kinetics. Adsorption is commonly used due to ease of operation and handling, higher removal efficiency, cost-effectiveness, and adsorbent disposal properties. For effective adsorption, the adsorbents must possess the characteristics such as greater removal efficiency, adsorption capacity, cost-effectiveness, disposal safety, and greater surface area. In this situation, a media's porosity and pore size distribution are even more crucial to improve the adsorbent's overall efficiency in removing arsenic. Graphene oxide (GO) has gained more attention increases for eliminating heavy metals from contaminated water and waste water stream due to its exceptional physicochemical properties like specific specific area, presence of hydroxyl, epoxy, and carboxyl groups such properties improve its ability to binds with metal ions through adsorption processes such as electrostatic attraction, ion exchange also shows a strong attraction for As^{3+}, and As^{5+} due to the existence of negatively charged oxygen functional groups [Thangavel et al., 2015; Tewari et al., 2022]. Graphene oxide doped in geopolymer used as an adsorbent to decontaminate the water, due to the two dimensional semi-planar architecture of Graphene oxide to oxygenated functional groups which are linked using covalent bonds and oxygen atoms across the carbon structure. These functional groups encompass hydroxile (-OH), epoxy (C-O-C), carboxile (COOH), as well as carbonile (C = O). In these way functional groups increases the surface area and provide adsorption sites which increase adsorption capacity. Graphene oxide strongly binds with heavy metals such as As with binding energy of -4.5 eV and also capable to capture arsenic species directly affected by oxidation [Liao et al., 2022: Gopalakrishnan et al., 2015]. In this effort, a versatile class adsorbent having effective, economical made by graphene oxide mixed with sodium based geopolymer, silicon metal powder was added as pore forming agent strong mechanical backing for sequestration heavy metals from underground and surface water. However, limited work has been reported conclusively in order to show that the base media's porosity and pore size distribution have a significant impact on the metal hydroxide sequestration. Moreover, the greater porosity minimizes the constraints on intra particle mass transport, thereby enhancing the overall kinetic efficiency of the system. Additionally the mechanism and performance of the porous Na-geopolymer adsorbent were assessed through adsorption isotherm and kinetic modeling for the validation of experimental results by renowned Freundlich and pseudo second order kinetic model.

MATERIALS AND METHOD

Chemicals and reagents

Sodium hydroxide pellets were reagent grade, 99% purity purchased from Ward's Science (New York, USA). Silicon metal powder, 99.9% purity, was purchased from Alfa Aesar Johnson Matthey Company (Massachusetts, USA). Silicon nanopowder, 30–50 nanometer average particle size, 98% purity, was purchased from

Nanostructured and Amorphous Material, Inc. (Houston, Texas, USA). Metakaolin Metamax EF with an average particle size of 2.66 µm was purchased form BASF GmbH Germany.

Preparation of porous geopolymer adsorbent

Sodium silicate and geopolymer pastes were prepared by procedures [Davidovits, 2017; Böke et al. 2015]. The process involved weighing and adding sodium silicate to a polyethylene PE container, initiating mechanical mixing using an IKA Eurostar Digital Mixer Cole-Parmer, IL-USA at 400 rpm with high torque. Metakaolin powders were gradually introduced during this phase to prevent sudden water uptake and clogging. After 1 minute of mechanical mixing, high shear mixing commenced at 2000 rpm to create a vortex and efficiently form slurry by mixing the powders with water. Following an additional 7 minutes of shear mixing, graphene oxide nanoparticle and metal powders with desired particle sizes and weight percentages were incorporated and mixed for an additional two minute, resulting in a total mixing time of 10 minutes. The geopolymer slurries were cast into plastic cylindrical molds with a diameter of 30 mm, sealed with a polymer lid, and matured at 50 °C for 24 hours in an electric oven Carbolite Furnace, USA under 90% relative humidity. As anticipated, the formation of pores and expansion in the mold occurred vertically as water evaporated and condensed on the upper walls of the mold.

Characterization of porous geopolymer using various analytical technique

The synthesized samples underwent XRD analysis using a diffractometer (BRUKER D8-ADVANCE, Germany) equipped with a θ–2θ Bragg-Brentano geometry detector and tube. The XRD analysis covered the range of 5–70° in 2θ, employing a 40 kV accelerating voltage and 40 mA beam current. The analysis used 0.027 step sizes and operated at a speed of 0.1°/sec. To enhance sample representation and optimize the signal, the synthesized Na-geopolymer composites were pulverized to 200 µm powder sizes using a mortar and pestle before being loaded onto the XRD stage. Surface properties such as specific surface area, pore size, and pore volume distribution were examined using the Brunauer-Emmett-Teller (BET) method in a nitrogen adsorption and desorption environment with ASAP 2020 PLUS-Micrometrics. The synthesized materials were ground and degassed overnight at 100 °C, and adsorption isotherms were recorded at 77 K. For microstructural analysis, the SEM played a crucial role. The SEM, specifically the Axis-ChemiSEM, is a versatile instrument for analyzing the microstructural characteristics of solid materials. It achieves high resolution by scanning the sample surface with a focused electronic beam, and interactions with sample atoms generate signals providing information about morphology and composition. The SEM examination attains precision exceeding 1 nm and can operate in various conditions, including vacuum, low pressure, and low or high temperatures. The samples prepared for electron microscopy were carefully ground, sieved to a size of 300 µm, and placed in the sample holder to facilitate microstructural analysis.

Adsorption experiments

The effect of main parameter's pH, adsorbent dose and contact time was studied in this study. In 50 mL conical flasks, 20 mL of aqueous arsenic solution was subjected to adsorption experiments. Following the adsorption process, the suspension underwent filtration using a 0.22 mm syringe filter. 2% nitric was used to acidify filtrate and ICP-MS was used to determine elemental arsenic concentration. The adsorption capacity of arsenic adsorbed by porous geopolymer was determined using following relation.

$$q = \frac{Co - Ce}{m} \times V \tag{1}$$

where: q represents the amount of arsenic adsorbed by porous Na-GP (mgAs/gNa-GP), C_0 stands for the initial concentration of arsenic before the adsorption process (mg/L), Ce is the equilibrium arsenic concentration after the adsorption process (mg/L), m denotes the mass of the adsorbent (mg), and V defines the volume of the solution (L).

Adsorption efficiency can be expressed by given equation.

$$Adsorption\ efficiency = \frac{Co - Ce}{Co} \times 100 \tag{2}$$

The time for collection of samples was set to start from 20 minutes with an interval of 20 minutes and continues till 240 minutes of experiment. For the adsorption isotherm plots different amounts (0.1, 0.25, 0.5, 0.75, and 1.0 g) of porous Na-GP were added to arsenic species solutions separately, and the system was allowed to equilibrate for 60 minutes. To explore the impact of adsorbent dosage on the uptake of various arsenic species, different amounts of the adsorbent were introduced into the solution.

RESULTS AND DISCUSSIONS

Porous geopolymer samples were subjected to comprehensive characterization using multiple analytical techniques. For analysis of surface of porous geopolymer formed at micro-level analysis of surface the techniques used were SEM as shown in Figure 2 and BET analysis was employed to measure pore size, pore volume, and specific surface area. The ensuing results are presented and discussed below

Effect of dopant on morphology NaGP

Figure 2 illustrates the morphological aspects of synthesized porous Na-geopolymer samples incorporating a pore-forming agent. Microstructural analysis and porosity characterization were conducted using scanning electron microscopy, with silicon (Si) metal powder of 150 micrometer size acting as the pore former. The samples, treated at 50°C and 70% relative humidity for one day, were examined with varying percentages (1 wt%, 3 wt%, and 5 wt%) of silicon metal powder. The influence of silicon metal powder content on the pore structure was observed, indicating a direct correlation. With an increasing amount of Si metal powder, the geopolymer material exhibited larger pore diameter, increased pore volume, and a transition from thick to thin pore walls. For samples with 1 wt% silicon metal powder doping (Fig. 1a), small, regular, and uniform pores with thin walls were observed. The fine pore structure inside displayed interconnectivity. The addition of 3 wt% metallic silicon at 50 °C led to an increase in pore size and volume, accompanied by a gradual decrease in specific surface area (Table 1), resulting in larger pores (Fig. 1b). Further increasing the amount of silicon to 5 wt% resulted in the

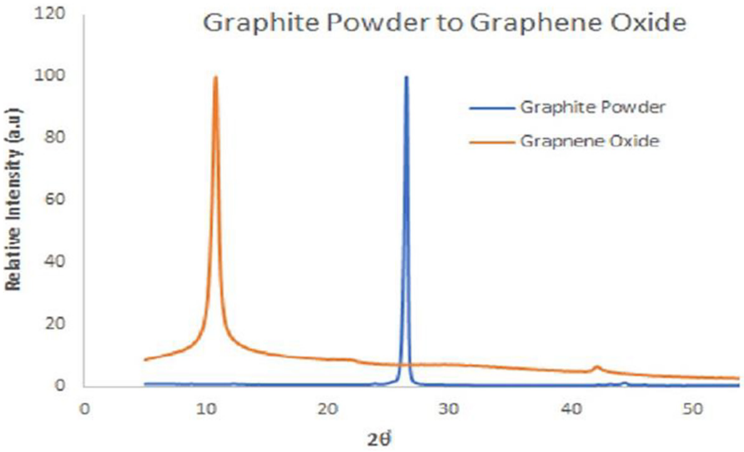

Figure 1. XRD patterns of GO doped NaGP

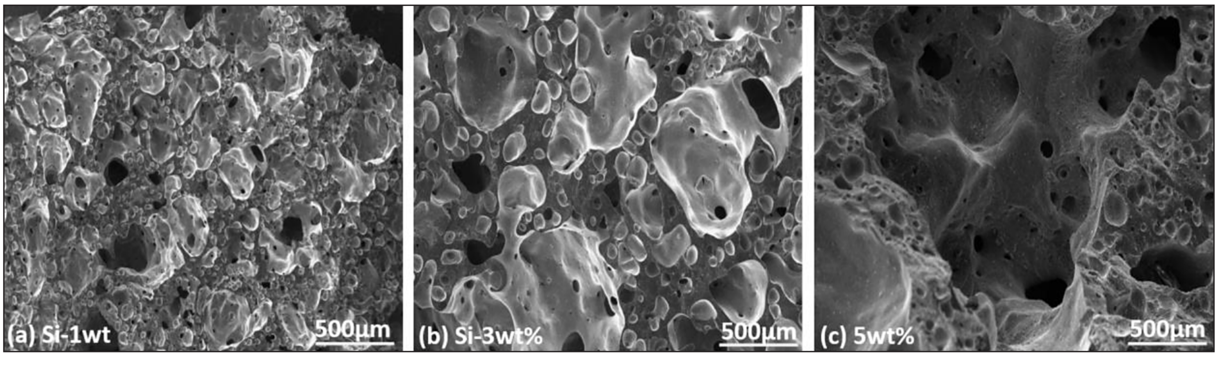

Figure 2. Morphology of porous Na- geopolymer formed by varing %age of metalic silicon powder of size (150 µm) with addition (a) Si-1wt%, (b) Si-3wt% (c) Si-5wt% in at 50 °C

formation of larger and uncontrollable pores due to increased H2 gas production within the geopolymer matrix (Fig. 1c and Equation 1). Equations depicting the potential reactions induced by the addition of metallic silicon in the Na-geopolymer matrix to form pores and aid in the geopolymer's maturation are provided.

$$Si + 4H_2O \leftrightarrow Si(OH)_4 + 2H_2 \uparrow \qquad (3)$$

$$Si(OH)_4 \leftrightarrow SiO_2 + 2H_2O(\text{aq}) \qquad (4)$$

Effect of dopant on surface area and pore features of geopolymer (BET)

Figure 3 illustrates N_2 adsorption/desorption isotherms, while Table 1 outlines the properties of porous geopolymer with varying percentages of incorporated silicon metal powder. Notably, the sample with 1% Si addition displayed the highest BET surface area (34.4596 m²/g). Conversely, samples with 3% Si addition (12.5147 m²/g) and 5% Si addition (1.492 m²/g) exhibited lower values. All three adsorption/desorption isotherms conform to type IV, according to the IUPAC classification, as depicted in Figure 3. The detailed particulate surface properties, including surface area, pore size, and volume distribution, are consolidated in Table 01. With an increasing addition of silicon, both BET surface area and porosity decrease. In contrast, there is an inverse correlation observed in pore size and pore volume concerning the samples (1%Si-Na-GP, 3%Si-NaGP, 5%Si-NaGP). This trend is corroborated by SEM analysis Figure 1, indicating that the escalating addition of silicon induces more H_2-gas production within the geopolymer matrix. Consequently, this phenomenon contributes to the decrease in surface area and porosity while concurrently increasing pore size and pore volume.

Effect of curing temperature over structure of Na-geopolymer (XRD)

The samples were produced by incorporating optimized silicon at 1 wt% and then cured at different temperatures, specifically 30 °C, 50 °C, and 70 °C, for a time of 24 hours. Subsequently, the samples were left outside for three days until a constant mass was achieved. Figure 4 illustrates the effect of varying curing temperatures on the behavior of samples with 1 wt% Si addition during the construction of the geopolymer matrix. The peaks observed at 25.1°, 47.58°, 54°, 55°,

Table 1. The characteristics of porous geopolymer with the incorporation of silicon metal powder at an optimized temperature of 50 °C are as follows

Samples	BET surface area (m²/g)	Pore size Å	Pore volume (cm³/g)	Porosity
Na-GP+1%Si	34.4596	103.822	0.0731	73.304
Na-GP+3%Si	12.5147	114.382	0.075	61.3449
Na-GP+5%Si	1.492	141.931	0.077	57.585

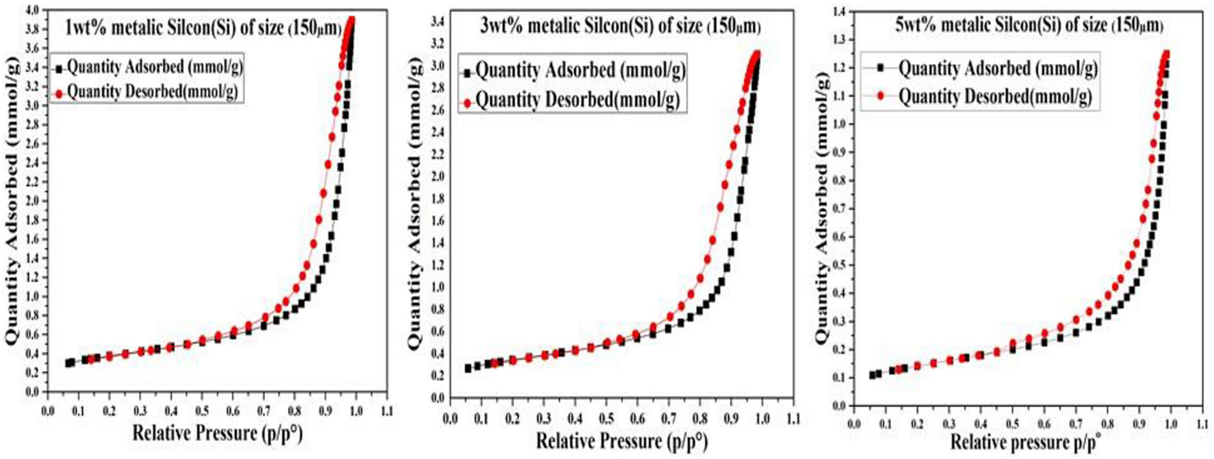

Figure 3. N_2-gas adsorption desorption isotherm curve of smaples (a) 1wt% (Si) (b) (3wt%)(c) and (5wt%) metalic silcon optimed tepmerature 50 °C

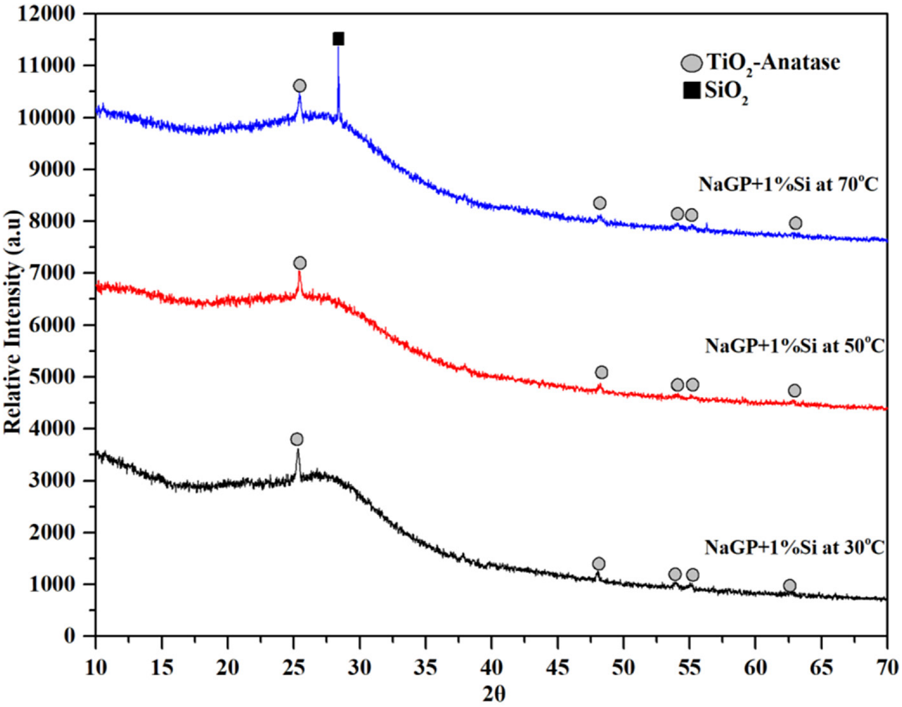

Figure 4. XRD patterns of NaGP along with 1wt % Si-150 µm powder additions at 30 °C, 50 °C, and 70 °C

and 62.5° (2θ) angles at temperatures of 30 °C, 50 °C, and 70 °C suggest the presence of TiO_2 as a crystalline impurity originating from the base material metakaolin. When curing temperature is enhanced, no significant change was observed up to 50°C, indicating the formation of an amorphous phase. This suggests that all the silicon powder in the geopolymer matrix was utilized to produce amorphous silica (SiO_2), contributing to the continuous geopolymerization reaction chain. As the temperature reaches 70 °C, another peak of SiO_2 at 28.2° (2θ) angles emerges, indicating the presence of unreacted silica left behind due to the evaporation of the alkaline phase

FTIR analysis of porous Na-geopolymer

The Fourier Transform Infrared (FTIR) analysis of porous Na-geopolymer powders was conducted employing the KBr pelletizing technique. This technique facilitated the transmission of peaks through transparent pellets, creating distinct phases with coincident waves. The transmittance values obtained were normalized, and the identified peaks were examined to better understand the structural variations arising from varying levels of silicon additions. Figure 11 presents the FTIR spectra of three specific samples, each with 1wt%, 3%, and 5 wt% Si additions, respectively.

In the FTIR spectra of porous Na-geopolymer illustrated in Figure 5, the incorporation of silicon (Si) reveals prominent water peaks within the wavenumber range of 3456 cm^{-1} and 1642 cm^{-1}. These specific wavenumbers correspond to the OH bonds present in the Na-geopolymer, offering insights into the hydration state and the environment of the charge-balancing cations [Sauffi et al. 2022)]. Additionally, a distinct peak at 3456 and 1642 cm^{-1} corresponds to the stretching and bending vibrations of OH and H-O-H molecules within the geopolymer matrix. With the introduction of 3% and 5 wt% Si, the 1019 cm^{-1} peak is intensified compared to the 1wt% Si addition, indicating increased NASH formation with a deeper O-Si-O bending peak at 451 cm^{-1} in the fingerprint range. This suggests a higher Si contribution to the amorphous phase, generating disiloxo and siloxo-sialate groups for continued polymer chain reactions. This enhancement is associated with the creation of larger and more open network pores, implying a potential increase in water content. The infrared spectrum of porous geopolymer highlights a main absorption band at 1019 cm^{-1}, corresponding to the symmetric stretching vibration of Si-O-Si and Si-O-Al bonds in SiO_4 and AlO_4 tetrahedral within the geopolymer network. The absorption band at 1384 cm^{-1} signifies the stretching vibrations of C-O bonds of CO_3^{2-} ions,

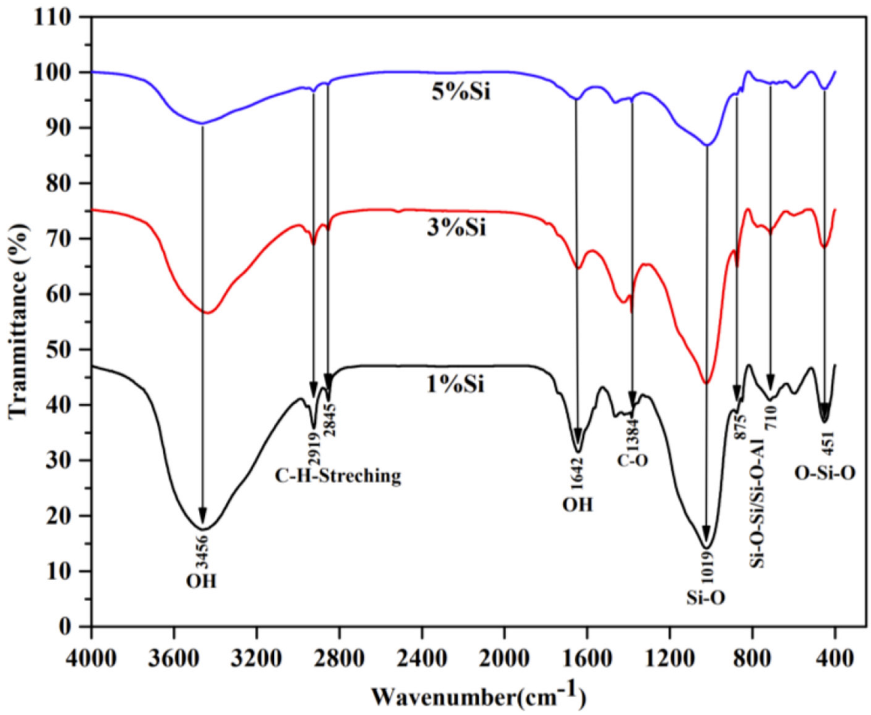

Figure 5. FTIR analysis of porous Na-geopolymer with 1wt %, 3, wt% and 5% additions

a result of the reaction between atmospheric CO_2 and residual sodium content. Post-geopolymerization, the band shifts to lower wavenumbers (875–710 cm^{-1}), indicating the formation of a silicate geopolymer network with higher cross-linking and larger molecular structures [Lemougna, MacKenzie, and Melo 2011; Sauffi et al. 2022]. The absorption bands in the Fourier Transform Infrared Spectra (FTIR) are summarized in the provided Table 2.

In Figure 4, the densities of the synthesized samples were determined using Archimedes' principle water immersion technique to estimate apparent porosity and density. As depicted in Figure 7, the addition of Silicon (Si) at 1wt%, 3wt%, and 5wt% leads to a decrease in density, attributed to the formation of larger pores as explained earlier in Figure 2. Simultaneously, the temperature exhibits a direct proportionality to apparent porosity, which increases with the temperature rise. At an initial applied temperature of 30°C, the observed porosity was 15%, and this increased to 75% at 50 °C due to a greater production of H_2 gas. Further temperature increase to 70 °C resulted in a slower trend, attributed to the evaporation of the alkaline phase from the matrix. This leads to a slowdown in the reaction rate and H_2 gas production, allowing the reaction to proceed continuously.

Effect of pH

The influence of pH on the adsorption of arsenic (III) and arsenic (V) onto porous Na-GP was investigated by altering the pH within the range of 5 to 10. Various pH solutions were prepared by incrementally adding dilute NaOH or HNO_3 solutions to attain the desired pH values.

The Figure 6 reveals that the efficiency of arsenic (III) removal increases with increasing pH from 5 to 6 after that the marginal decrease was

Table 2. Fourier transform infrared spectra of porous Na-geopolymer

Band (cm^{-1})	Assignment
3456 cm^{-1}	Vibration of OH^{-} group of porous Na-geopolymer
1642 cm^{-1}	OH-bending vibration of H-O-H
1384 cm^{-1}	Stretching vibration of CO_3
1019 cm^{-1}	Stretching vibration of Si-O-Si and Si-O-Al
875-710 cm^{-1}	4-Coordinated Al-O bond

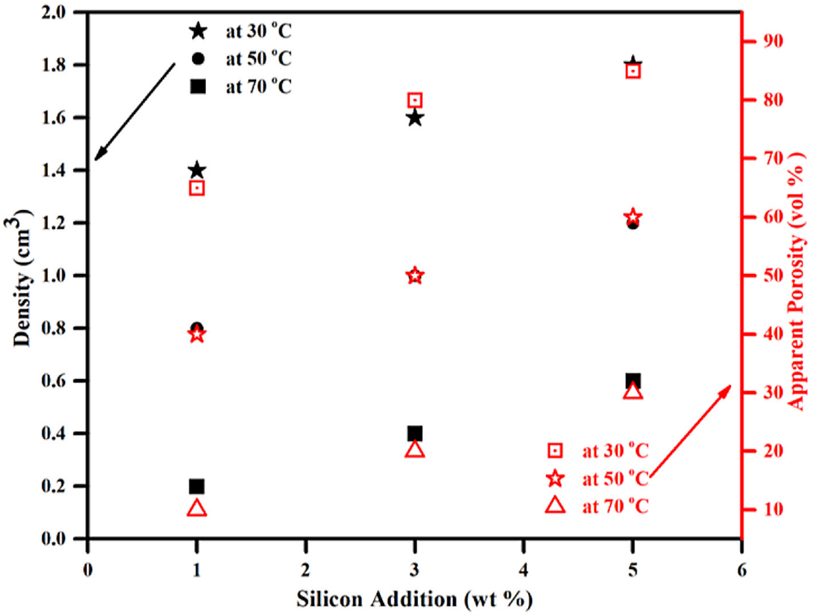

Figure 6. Effect of temperature and silicon addition on density and apparent porosity at 50 °C

observed. In case of arsenic (v) highest removal was achieved at pH range from 8 to 9.5. The pH of solution has main impact on surface charge of adsorbent and ionization of arsenic specie. Surface charge of adsorbent best understood by pH of point of zero charge [Wimalasinghe et al., 2018]. The pH_{pzc} of 6 was obtained, it gives information about surface of the charge that it is negative if pH is greater than 6 and positively charged if pH is less than 6. The grapheme oxide on exposure to water attract hydroxyl group or release H+ depend on pH [Siddiqui, S. I, et. al 2017]. The presence of As (V) is in pH range of 5 to 6 in form of $HAsO_4^{2-}$ and AsO_4^{3-} and pH 6-12 unfavorable more for As(V) adsorption. The hydroxyl surface charge attach with hydrogen ions at lower pH there is favorable chance of bonding of As(V) and grapheme oxide doped geopolymer and at greater alkaline pH surface become negatively charged so un-favorable for As(V) adsorption. As shown in Figure 7 adsorption

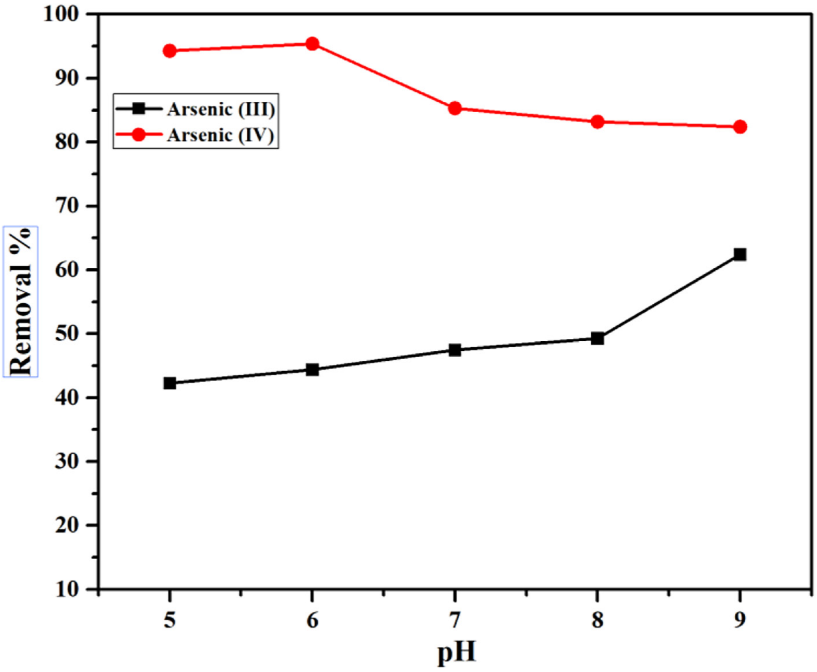

Figure 7. Effect of pH on Arsenic uptake (50 ppb concentration, 25 °C, dose = 1.0 g, and contact time = 60 min)

of As (III) slowly enhances from pH 5 to 8 afterwards raptly increased at greater than pH 10.

Effect of initial concentration and treatment time

The adsorption efficiency declined from 62 to 16 %, 94 to 31% for As(III) and As(V) with an increment in the initial concentration of arsenic species from 50 mg/L to 120 mg/L as shown in Figure 5. The concentration of As (V) remains constant after 120 mg/L. The decrease in adsorption efficiency after certain time is due to fixed amount adsorbent has fixed quantity of adsorbates to be adsorbed and initially it is greater after wards it decreases. Figure 8 shows that at the start of experiment the removal efficiency was greater and slowly decrease and it became to reach to equilibrium after 60 minutes, Since initially there are greater pores in adsorbent to adsorb the arsenic species and afterwards when experiment continues the pore start to become saturated after certain time there will no space in surface of adsorbent to adsorb. Several investigations have shown decrease in initial concentration of pollutant lead to increase removal efficiency.

Effect of dosage

The adsorbent dose of 0.1 gm was increase to 1 gm to see the effect of adsorbent dose on removal performance for arsenic. However the volume of solution was 50 ml and arsenic concentration of 10 mgL. By increasing the dose from 0.1 to 1 gm. adsorption efficiency increased from 12 to 62% and 32 to 94% for As(III) and As(V) respectively with enhances adsorbent amounts from 0.1 to 1 gm. The behavior of increase in removal efficiency of arsenic species was due to greater active sites present at higher adsorbent dose and As(V) has greater interaction with grapheme oxide doped geopolymer so it has greater removal compared with As(III).

Adsorption isotherm

Adsorption isotherms provide the relation among the molecules of adsorbates and active sites on adsorbent surface. They are instrumental in explaining the correlation among the quantity of adsorbates, adsorbent and concentration remains in the solution at a constant temperature. In this research, equilibrium data related arsenic adsorption underwent analysis by Freundlich model (1906). The Langmuir isotherm and Freundlich isotherm models, normally employed in describing solid-liquid systems, offer distinct approaches. The Langmuir model can be expressed in the following form:

$$\frac{Ce}{Qe} = \frac{Ce}{Qm} + \frac{1}{bqm} \tag{5}$$

Following equation is of Freundlich isotherm model.

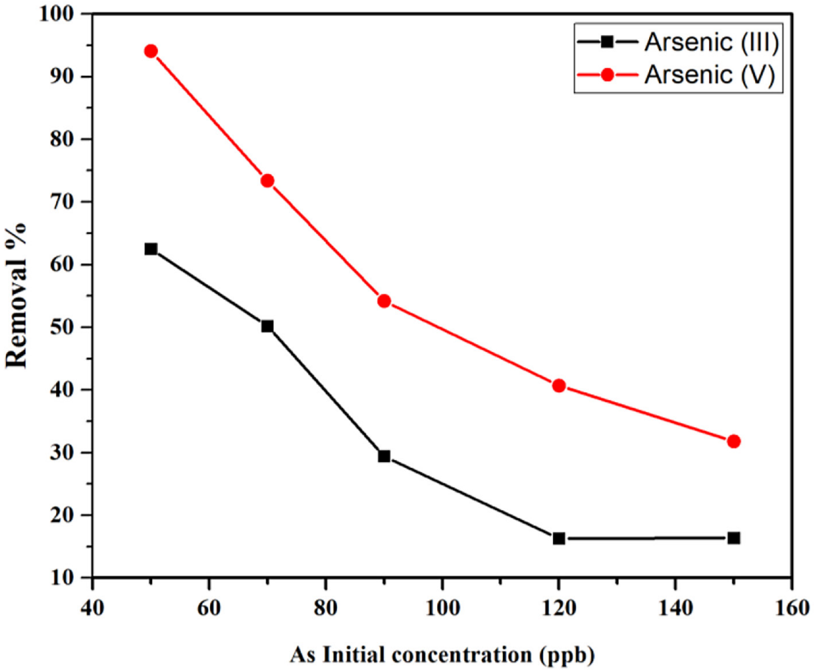

Figure 8. Effect of initial concentration on As(V) and As(III) removal at optimized operating conditions

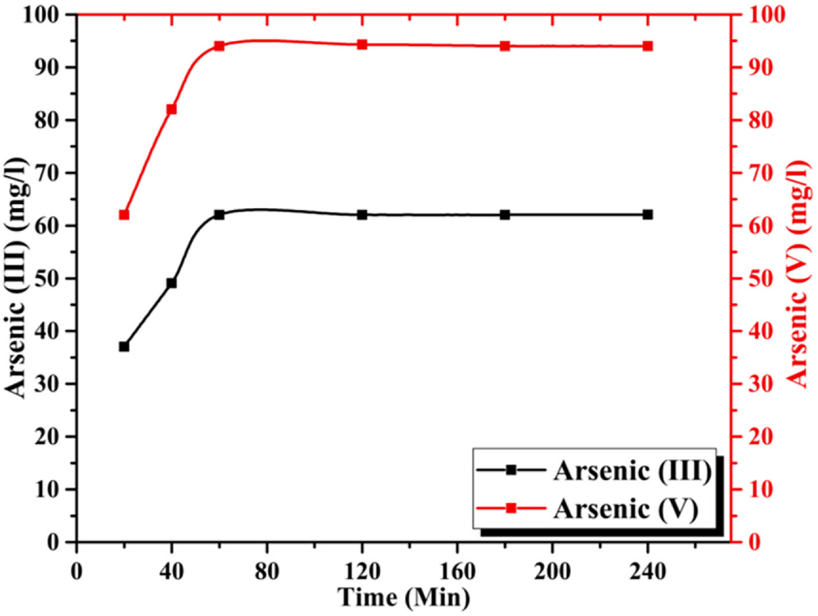

Figure 9. Effect of treatment time on As(V) and As(III) removal at optimized operating conditions

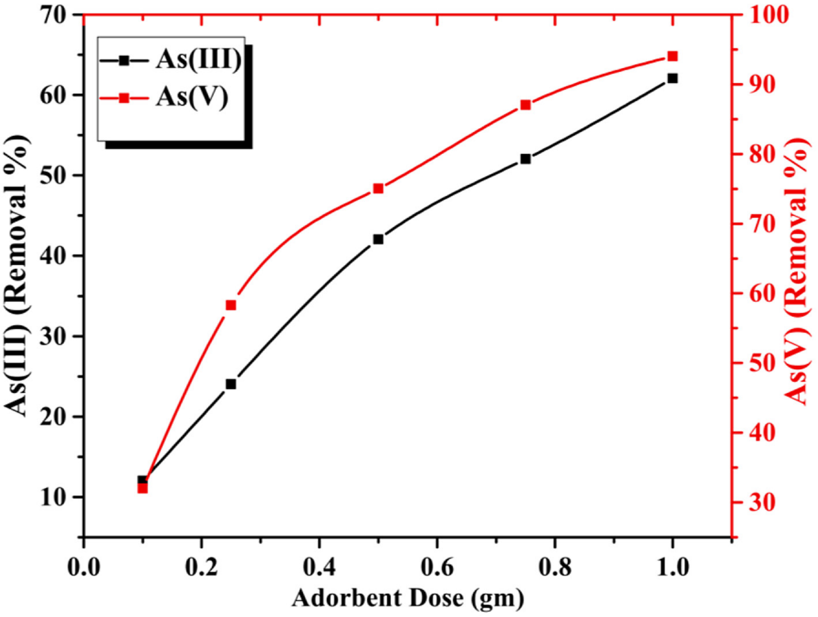

Figure 10. Effect of adsorbent dosage on Arsenic uptake (50 ppb concentration, 25 °C, pH = 5 for for for As(V) and As (III) 9.5 contact time = 120 min)

$$Logqe = \frac{1}{n}\ Logqe\ +\ LogKf \qquad (6)$$

where: *Ce* shows the equilibrium concentration (mg/L), *qe* represents the amount of arsenic adsorbed at equilibrium while *qm* is the maximum of arsenic adsorbed on the porous geopolymer adsorbent surface, *b, Kf*, *n* considered as Langmuir equilibrium constant and Freundlich constants respectively, indicating the intensity and relative adsorption capacity of the adsorbent in adsorption process.

$$qm = KfC_0^{\frac{1}{n}} \qquad (7)$$

R_L, I is dimensionless quantity shows in Equation 4 which favors the adsorption process

$$R_L = \frac{1}{1 + BC_0} \qquad (8)$$

From correlation coefficients study discloses that the adsorption by porous geopolymer exactly explained by Freundlich isotherm model, which indicates that nature of adsorbent, was heterogeneous and multilayer adsorption. The values of n>1 suggested that good connection among the adsorbent and adsorbates [Tian and Sasaki, 2019]. Therefore, the interface power of both As(V) > As(III) through porous geopolymer follows the order of. The 1551 and 2351 µg/g As(III) and As(V) maximum adsorption capacity (qm) were achieved using Freundlich isotherm model respectively, ambient temperature. The rate of adsorption on porous geopolymer adsorbent were demonstrated by pseudo-second-order Equation 5

$$\frac{\mathrm{t}}{\mathrm{qt}} = \frac{1}{\mathrm{Kq_e^2}} + \frac{1}{\mathrm{qe}}\mathrm{t} \tag{9}$$

where: *qt* (mg g^{-1}) and *qe* (mg g^{-1}) are adsorption capacities on time t and equilibrium time h (mg g^{-1} min^{-1}) represents the initial sorbate rate, while k (g mg^{-1} min^{-1}) shows the rate constant of adsorption, can be defined as

$$h = kq_e^2\ t \rightarrow 0 \tag{10}$$

Figure 6 represents the kinetic plots both arsenic species at optimized values. The $R^2 = 0.9686$ and 0.9496 for As(III), As(V) obtained respectively, which show better kinetics of arsenic adsorption on porous geopolymer well fits by pseudo-second-order kinetic model. This specifies that adsorption is well-ordered by chemisorption described. The Table 3 represents the values of h, k and R^2 for arsenic As(V), As(III) respectively which are directly proportional to the adsorption while initial concentration was inversely proportional rate constants as initial concentration rate constant decreased which revealed that adsorption of arsenic on porous geopolymer adsorbent was slower with increasing initial concentration.

Table 3. Freundlich isotherm parameters for As(III), As(V) at ambient temperature

Arsenic	n^a	K_f^b(mg$^{1-1/n}$L$^{1/n}$g^{-1})	q_m^c (mg/g)	R^2
As (III)	1.316	0.161	1.505	0.9686
As (V)	1.942	1.196	2.098	0.9496

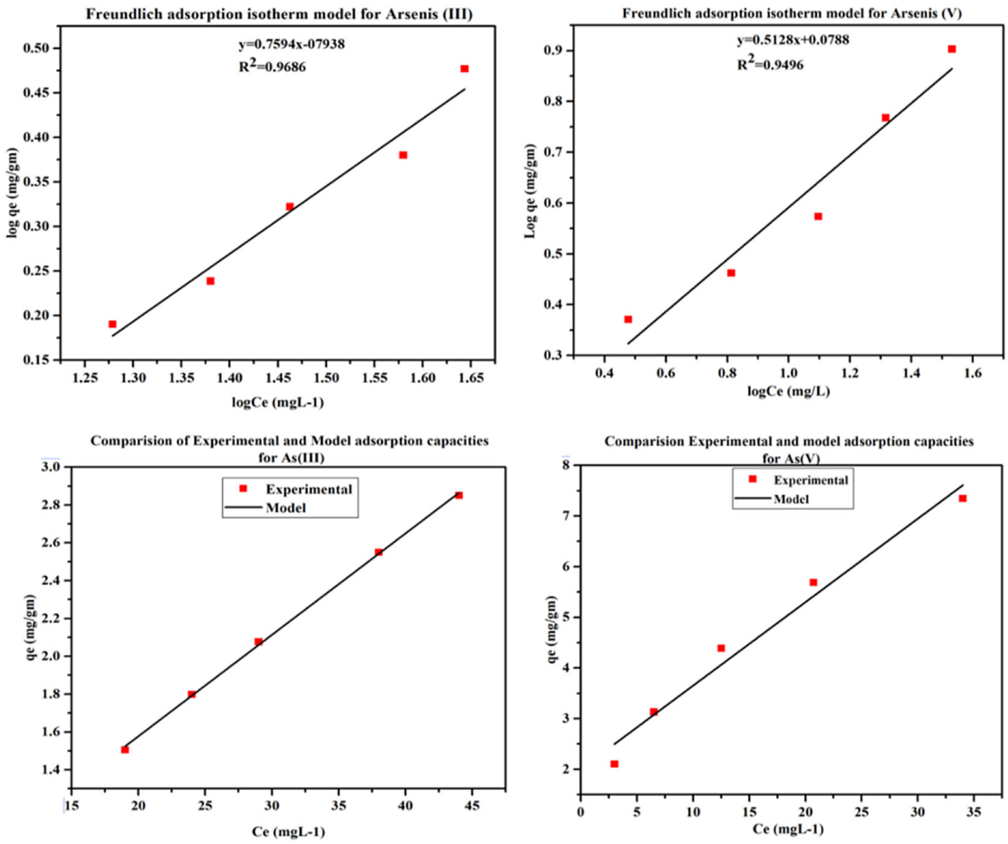

Figure 11. Freundlich Adsorption isotherm fitting for efficient adsorption of As(III) and As(v) on adsorbent

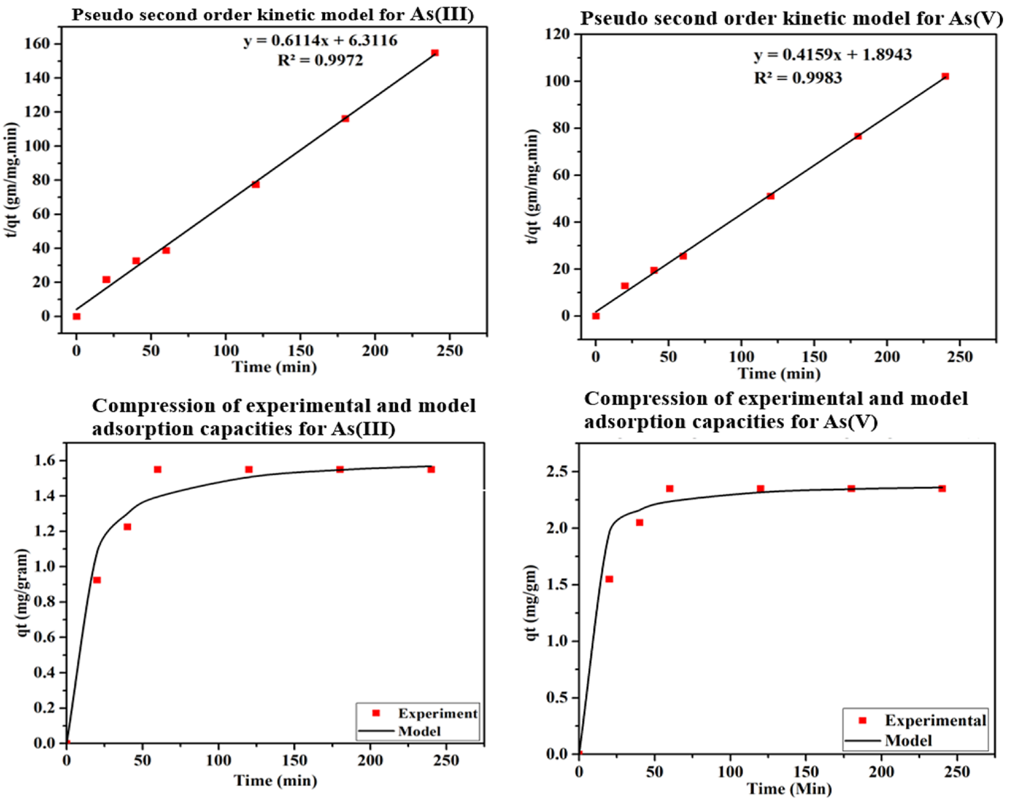

Figure 12. Kinetic study of adsorption for removal of As(III) and As(V)

Table 4. Validation of results with other researchers

Geopolymer adsorbent	Equilibrium time (h)	Adsorption isotherm	Adsorption capacity		References
			As (III) µg/g	As(V) µg/g	
Graphene oxide doped geopolymer	1	Freundlich	1551	2351	This study
Iron oxide-modified nonporous geopolymers	72	Freundlich	950 µg/g	-	Medpelli et al. (2015)
Iron oxide coated geopolymer microspheres	1	Freundlich	614.4	1689.	Nimisha Thakur et al. (2021)
Fe(II)-modified geopolymer	24	Freundlich	-	-	Tian and Sasaki (2019)

Note: n^a is Freundlich constant, dimensionless quantity and intensity of adsorption process, Kf^b is the Freundlich constant indicates the relative adsorption capacity used adsorbent, qm^c represents the the maximum quantity of arsenic attached on the adsorbent surface (mgAs/g Na-GP). When the $R_L = 0$ (irreversible), $R_L = 0 < 1$ (favorable), $R_L = 1$ (linear) and $R_L > 1$ (unfavorable). The RL values recent study shows higher than 0 and lower than 1 which shows the favorable adsorption.

CONCLUSIONS

A significant and successful effort was undertaken to fabricate porous geopolymers by incorporating varying weight percentages of dopant to customize the pore size and wall thickness of geopolymer frameworks. The introduction of 1 wt% of Si resulted in the formation of spherical interconnected pores within the geopolymer, achieving maximal surface area and porosity. Temperature exerted a positive influence on pore formation due to increased vapor pressure of water and humidity in the oven, promoting enhanced interaction with the alkaline medium. An elevated Si concentration favored pore formation, particularly at 50 °C. Adsorption test was conducted successfully for arsenic metal ions concentration using porous geopolymer adsorbent. The various process parameter such as initial arsenic concentration of influent, pH of solution, retention time and adsorbent dose. The maximum adsorption capacity was obtained at a pH-6 and 9 for arsenic (V) and arsenic (III) at, contact time 120 min, adsorbent dose of 1 g/L and Initial concentration of 50 ppb. The 1551 µg/g, 1551 µg/g adsorption capacity and (0.9686) and (0.9496) R^2 for both arsenic type As(III), As(V) was obtained by well-known Freundlich isotherm model accorded well with pseudo-frst-order kinetics, respectively. Further it concluded that synthesized adsorbent has a great potational for the removal heavy metal action's specially As (III) and As (V) due to their high surface area, porosity and spherical particle shape. This investigation lays the groundwork for synthesizing porous geopolymers with potential applications in nano/micro membranes for groundwater, surface, as well as wastewater treatment.

Acknowledgements

This research work was highly acknowledged by International Research Support Initiative Program (IRSIP) from the Higher Education Commission of Pakistan for six month and then for further six month was funded by a Congressional Mandate Grant to the U.S. Army Corps of Engineers, Engineer Research Development Corps (ERDC), through the Construction Engineering Research Laboratory (CERL) in Champaign, Illinois. The authors acknowledge the use of facilities in the Center for Microanalysis of Materials, as part of the Frederick Seitz Materials Research Laboratory at the University of Illinois at Urbana-Champaign.

REFERENCES

1. Al- Zeer, Mohammad I.M. Al, and Kenneth J.D. Mackenzie. 2019. Fly ash-based geopolymers as sustainable bifunctional heterogeneous catalysts and their reactivity in friedel-crafts acylation reactions. Catalysts 9(4). https://doi.org/10.3390/catal9040372
2. Unis A.H., Mohammed A.S., Qaidi S.M.A., Faraj R.H., Sor N.H., and Mohammed A.A. 2022. Compressive strength of geopolymer concrete composites: a systematic comprehensive review, analysis and modeling. European Journal of Environmental and Civil Engineering 27(3), 1383–1428. https://doi.org/10.1080/19648189.2022.2083022
3. Alzeer M.I.M., MacKenzie K.J.D., and Keyzers R.A. 2016. Porous aluminosilicate inorganic polymers (Geopolymers): A new class of environmentally benign heterogeneous solid acid catalysts. Applied Catalysis A: General 524, 173–81. https://doi.org/10.1016/j.apcata.2016.06.024
4. Asia, South, and Sarker B. 2021. Scientific review surface and ground water pollution: causes and effects of surface and ground water pollution: causes and effects of urbanization and industrialization in South Asia," no. July. https://doi.org/10.32861/sr.73.32.41
5. Bhatti, Z.A., Qureshi K., Maitlo G. Technology Karachi, Shoaib Ahmed, and Technology Karachi. 2020. Study of PAN Fiber and Iron Ore Adsorbents for Arsenic Removal, no. March. https://doi.org/10.28991/cej-2020-03091491
6. Böke, N., Birch G.D., Nyale S.M., and Petrik L.F. 2015. New synthesis method for the production of coal fly ash-based foamed geopolymers. Construction and Building Materials 75, 189–99. https://doi.org/10.1016/j.conbuildmat.2014.07.041
7. Cai, B., Engqvist H., and Bredenberg S. 2014. Evaluation of the resistance of a geopolymer-based drug delivery system to tampering. International Journal of Pharmaceutics 465(1–2), 169–74. https://doi.org/10.1016/j.ijpharm.2014.02.029
8. Umejuru E.C., Mashifana T., Kandjou V., Amani-beni M., Sadeghifar H., Fayazi M., Karimi-maleh H., and Thandiwe N. 2023. Application of zeolite based nanocomposites for wastewater remediation : evaluating newer and environmentally benign approaches. Environmental Research 231 (P1), 116073. https://doi.org/10.1016/j.envres.2023.116073
9. Chung, J.Y., Yu S.D., and Hong Y.S. 2014. Environmental source of arsenic exposure. Journal of Preventive Medicine and Public Health 47(5), 253–57. https://doi.org/10.3961/jpmph.14.036
10. Das S., Saha P., Jena S.P., and Panda P. 2022. Geopolymer concrete: sustainable green concrete for reduced greenhouse gas emission – A review. Materials Today: Proceedings 60, 62–71. https://doi.org/10.1016/j.matpr.2021.11.588
11. Davidovits, J. 2017. Geopolymers: Ceramic-like inorganic polymers. Journal of Ceramic Science and Technology 8(3), 335–50. https://doi.org/10.4416/JCST2017-00038
12. Davidovits J. 1994. Propertıes of Geopolymer Cements Joseph Davidovits Geopolymer Institute, 02100 Saint-Quentin, France, 1–19.
13. Davidovits J. 2002. 30 Years of Successes and Failures in Geopolymer Applications. Market Trends and Potential Breakthroughs. Geopolymer 2002 Conference, 1–16.
14. Grba, N., Baldermann A., and Dietzel M. 2023. Novel green technology for wastewater treatment : geo-material / geopolymer applications for heavy metal removal from aquatic media. International Journal of Sediment Research 38(1), 33–48. https://doi.org/10.1016/j.ijsrc.2022.08.002

15. Guzmán-Carrillo, H.R., Gasca-Tirado J.R., López-Romero J.M., Apátiga-Castro M., Luis, M. Rivera-Muñoz E., Pineda-Piñón J., Pérez-Bueno J.J., Feregrino-Montes C., López-Naranjo E.J., and Manzano-Ramírez A. 2021. Encapsulation of toxic heavy metals from waste crt using calcined kaolin base-geopolymer. Materials Chemistry and Physics 257(2000). https://doi.org/10.1016/j.matchemphys.2020.123745
16. Javed, K., Mahmood S., Ammar M., Abbas N., Shah M.Y., Ahmed T., and Mustafa G. 2023. Rice husk ash adsorbent modified by iron oxide with excellent adsorption capacity for arsenic removal from water. International Journal of Environmental Science and Technology 20(3), 2819–28. https://doi.org/10.1007/s13762-022-04390-7
17. Khan, K., Irfan M., Amin N.U., Jiang H., and Gul S. 2023. Synthesis and characterization of porous reduced graphene oxide based geopolymeric membrane with titanium dioxide coating for forward osmosis application. Chemosphere 313 (September 2022), 137480. https://doi.org/10.1016/j.chemosphere.2022.137480
18. Khatri, N., and Tyagi S. 2015. Influences of natural and anthropogenic factors on surface and groundwater quality in rural and urban areas. Frontiers in Life Science 8(1), 23–39. https://doi.org/10.1080/21553769.2014.933716
19. Kupwade-Patil, K., Allouche E.N., Islam R., and Gunasekaran A. 2014. Encapsulation of solid waste incinerator ash in geopolymer concretes and its applications. ACI Materials Journal 111(6), 691–700. https://doi.org/10.14359/51686834
20. Łach M., Pławecka K., Bąk A., Lichocka K., Korniejenko K., Cheng A., and Lin W.T. 2021. Determination of the influence of hydraulic additives on the foaming process and stability of the produced geopolymer foams. Materials 14(17). https://doi.org/10.3390/ma14175090
21. Lemougna P.N., MacKenzie K.J.D., and Melo U.F.C. 2011. Synthesis and thermal properties of inorganic polymers (geopolymers) for structural and refractory applications from volcanic ash. Ceramics International 37(8), 3011–18. https://doi.org/10.1016/j.ceramint.2011.05.002
22. Medpelli D., Sandoval R., Sherrill L., Hristovski K., and Seo D.-k. 2015. Iron oxide-modified nanoporous geopolymers for arsenic removal from ground water. Resource-Efficient Technologies 1(1), 19–27. https://doi.org/10.1016/j.reffit.2015.06.007
23. Ali, M.A.Z., Sanjayan J., and Guerrieri M. 2017. Performance of geopolymer high strength concrete wall panels and cylinders when exposed to a hydrocarbon fire. Construction and Building Materials 137, 195–207. https://doi.org/10.1016/j.conbuildmat.2017.01.099
24. Ng C., Alengaram U.J., Wong L.S., Mo K.H., Jumaat M.Z., and Ramesh S. 2018. A Review on microstructural study and compressive strength of geopolymer mortar, paste and concrete. Construction and Building Materials 186, 550–76. https://doi.org/10.1016/j.conbuildmat.2018.07.075
25. Novais, R.M., Pullar R.C., and Labrincha J.A. 2020. Geopolymer foams: An overview of recent advancements. Progress in Materials Science 109 (November 2019). https://doi.org/10.1016/j.pmatsci.2019.100621
26. Pacheco-Torgal F., Castro-Gomes J., and Jalali S. 2008. Alkali-Activated Binders: A Review. Part 2. About Materials and Binders Manufacture. Construction and Building Materials 22(7), 1315–22. https://doi.org/10.1016/j.conbuildmat.2007.03.019
27. Pokhrel D., and Viraraghavan T. 2008. Arsenic removal in an iron oxide-coated fungal biomass column : Analysis of breakthrough curves 99, 2067–71. https://doi.org/10.1016/j.biortech.2007.04.023
28. Ricciotti L., Occhicone A., Ferone C., Cioffi R., Tarallo O., and Roviello G. Sustainable Design of Geopolymer-Based Materials for Artistic and Restoration Pr Ep Rin t n Ot p Ee r r Ev We d Pr Ep t n p r R.
29. Rickard, W.D.A., and Van Riessen A. 2014. Performance of solid and cellular structured fly ash geopolymers exposed to a simulated fire. Cement and Concrete Composites 48, 75–82. https://doi.org/10.1016/j.cemconcomp.2013.09.002
30. Rocca, D.G.D., Peralta R.M., Peralta R.A., Rodríguez-Castellón E., and Moreira R.deF.P.M. 2021. Adding value to aluminosilicate solid wastes to produce adsorbents, catalysts and filtration membranes for water and wastewater treatment. Journal of Materials Science 56(2), 1039–63. https://doi.org/10.1007/s10853-020-05276-0
31. Sauffi, A.S., Ibrahim W.M.W., Abdullah M.M.A.B., Ibrahim M., Ahmad R., and Zaidi F.A. 2022. Phase analysis of different liquid ratio on Metakaolin/Dolomite Geopolymer. Archives of Metallurgy and Materials 67(1), 247–50. https://doi.org/10.24425/amm.2022.137497
32. Sekkal W., and Zaoui A. 2023. Thermal and acoustic insulation properties in nanoporous geopolymer nanocomposite. Cement and Concrete Composites 138 (January): 104955. https://doi.org/10.1016/j.cemconcomp.2023.104955
33. Sharma S., Medpelli D., Chen S., and Seo D.K. 2015. Calcium-Modified Hierarchically Porous Aluminosilicate Geopolymer as a Highly Efficient Regenerable Catalyst for Biodiesel Production.” RSC Advances 5(80), 65454–61. https://doi.org/10.1039/c5ra01823d
34. Shehata N., Mohamed O.A., Sayed E.T., Abdelkareem M.A., and Olabi A.G. 2022. Geopolymer Concrete as green building materials: Recent

applications, sustainable development and circular economy potentials. Science of the Total Environment 836(March): 155577. https://doi.org/10.1016/j.scitotenv.2022.155577

35. Shridhar K., Krishnatreya M., Sarkar S., Kumar R., Kondal D., Kuriakose S., Rs V. Chronic Exposure to drinking water arsenic and gallbladder cancer risk: Preliminary evidence from endemic regions of India, 8, 406–14. https://doi.org/10.1158/1055-9965.EPI-22-0926
36. Singh, B., Ishwarya G., Gupta M., and Bhattacharyya S.K. 2015. Geopolymer concrete: A Review of some recent developments. Construction and Building Materials 85, 78–90. https://doi.org/10.1016/j.conbuildmat.2015.03.036
37. Siyal, A.A., Shamsuddin M.R., Khan M.I., Rabat N.E., Zulfiqar M., Man Z., Siame J., and Azizli K.A. 2018. A review on geopolymers as emerging materials for the adsorption of heavy metals and dyes. Journal of Environmental Management 224 (May): 327–39. https://doi.org/10.1016/j.jenvman.2018.07.046
38. Su, Q., Yang S., He Y., Qin Z., and Cui X. 2020. Prepared self-growing supported nickel catalyst by recovering Ni (II) from metal wastewater using geopolymer microspheres. Journal of Hazardous Materials 389 (December 2019), 121919. https://doi.org/10.1016/j.jhazmat.2019.121919
39. Supamathanon N., Boonserm K., Lisnund S., Chanlek N., Rungtaweevoranit B., Khemthong P., Wittayakun J., and Osakoo N. 2021. Development of CaO supported on modified geopolymer catalyst for transesterification of soybean oil to biodiesel. Materials Today Communications 29 (May): 102822. https://doi.org/10.1016/j.mtcomm.2021.102822
40. Tang J., Liu P., Xue S., Li Y., Zhao Y., Huang K., and Liu Z. 2023. Optimization of coal fly ash-based porous geopolymer synthesis and application for zinc removal from water. Ceramics International 49(4), 5828–33. https://doi.org/10.1016/j.ceramint.2022.10.028
41. Thakur N., and Armstrong D.W. 2021. Arsenic sequestration by iron oxide coated geopolymer microspheres. Journal of Cleaner Production 291, 125931. https://doi.org/10.1016/j.jclepro.2021.125931
42. Wang S., Yu L., Huang L., Wu K., and Yang Z. 2021. Incorporating steel slag in the production of high heat resistant fa based geopolymer paste via pressure molding. Journal of Cleaner Production 325 (October): 129265. https://doi.org/10.1016/j.jclepro.2021.129265
43. Xu X., Yang Y., Wang G., Zhang S., Cheng Z., Li T., Yang Z., Xian J., Yang Y., and Zhou W. 2020. Chemosphere removal of heavy metals from industrial sludge with new plant e based washing agents. Chemosphere 246, 125816. https://doi.org/10.1016/j.chemosphere.2020.125816
44. Zhang Z., John L.P., Reid A., and Wang H. 2014. Geopolymer foam concrete: An emerging material for sustainable construction. Construction and Building Materials 56, 113–27. https://doi.org/10.1016/j.conbuildmat.2014.01.081
45. Zhu, Y., Ji S., Liang W., Li C., Nie Y., Dong J., Shi W., and Ai S. 2022. A low-cost and eco-friendly powder catalyst: Iron and Copper nanoparticles supported on biochar/geopolymer for activating potassium peroxymonosulfate to degrade naphthalene in water and soil. Chemosphere 303 (P2), 135185. https://doi.org/10.1016/j.chemosphere.2022.135185
46. Thangavel, S. Raghavan, N. Kadarkarai, G. Kim, S.J. Venugopal, G. 2015. Graphene-oxide (GO)–Fe_3+ hybrid nanosheets with effective sonocatalytic degradation of Reactive Red 120 and study of their kinetics mechanism. Ultrason. Sonochem 24, 123–131.
47. Tewari C., Tatrari G., Kumar S., Pandey S., Rana A., Pal M., Sahoo N.G. 2022. Green and cost-effective synthesis of 2D and 3D graphene-based nanomaterials from Drepanostachyum falcatum for bio-imaging and water purification applications. Chem. Engg J.Chem Engg. J. Adv, 10, 100265.
48. Liao Y., Lei R., Weng X., Yan C., Fu J., Wei G., Zhang C., Wang M., Wang H. 2022. Uranium Capture by a Layered 2D/2d niobium phosphate/holey graphene architecture via an electro-adsorption and electro catalytic reduction coupling process. J. Hazard Mater., 442, 130054.
49. Gopalakrishnan A., Krishnan R., Thangavel S., Venugopal G., Kim S.J. 2015, Removal of heavy metal ions from pharma-effluents using graphene-oxide nanosorbents and study of their adsorption kinetics. J.Ind.Engg. Chem 30, 14–19.